4-1-2020

Optimal sizing design and operation of electrical and thermal energy storage systems in smart buildings

Ali Baniasadi
Edith Cowan University

Daryoush Habibi
Edith Cowan University

Waleed Al-Saedi
Edith Cowan University

Mohammad A. S. Masoum

Choton K. Das
Edith Cowan University

See next page for additional authors

10.1016/j.est.2019.101186

Optimal Sizing Design and Operation of Electrical and Thermal Energy Storage Systems in Smart Buildings

Ali Baniasadi[1,], Daryoush Habibi[1], Waleed Al-Saedi[1], Mohammad A.S. Masoum[1], Choton K. Das[1], Navid Mousavi[1]

[a]*School of Engineering, Edith Cowan University (ECU), 270 Joondalup Drive, Joondalup, Perth, WA 6027, Australia*

[b]*Department of Engineering, Utah Valley University, Orem, UT 84058, USA*

Abstract

Photovoltaic (PV) systems in residential buildings require energy storage to enhance their productivity; however, in present technology, battery storage systems (BSSs) are not the most cost-effective solutions. Comparatively, thermal storage systems (TSSs) can provide opportunities to enhance PV self-consumption while reducing life cycle costs. This paper proposes a new framework for optimal sizing design and real-time operation of energy storage systems in a residential building equipped with a PV system, heat pump (HP), thermal and electrical energy storage systems. For simultaneous optimal sizing of BSS and TSS, a particle swarm optimization (PSO) algorithm is applied to minimize daily electricity and life cycle costs of the smart building. A model predictive controller is then developed to manage energy flow of storage systems to minimize electricity costs for end-users. The main objective of the controller is to optimally control HP operation and battery charge/discharge actions based on a demand response program. The controller regulates the flow of water in the storage tank to meet designated thermal energy requirements by controlling HP operation. Furthermore, the power flow of battery is controlled to supply all loads during peak-load hours to minimize electricity costs. The results of this paper demonstrate to rooftop PV system owners that investment in combined TSS and BSS can be more profitable as this system can minimize life cycle costs. The proposed methods for optimal sizing and operation of electrical and thermal storage system can reduce the annual electricity cost by more than 80% with over 42% reduction in the life cycle cost. Simulation and experimental results are presented to validate the effectiveness of the proposed framework and controller.

Keywords: `Demand response, PV self-consumption, residential building, battery storage, thermal storage, storage sizing.`

Nomenclature

Acronyms

$\dot{m}_{HP}$	Mass water flow rate of HP (L/min).
$\dot{m}_{td}$	Mass water flow rate through the building (L/min).
C_g	Cost of electricity purchased from grid ($).

*Corresponding author

c_p	Specific heat capacity of water (J/(g/°C)).
C_{BSS}	Capital, replacement, and maintenance costs of BSS ($).
C_{batt}	Capacity of BSS (kWh).
C_{HP}	Cost of HP power consumption ($).
C_{TSS}	Capital and maintenance costs of TSS ($).
I_s	Solar radiation (W/m^2).
I_g	Internal heat gain (kW).
$m_{TSS,0}$	Initial chilled/hot water volume stored in TSS (L).
m_{TSS}	TSS stored chilled/hot water volume (L).
P_{ch}	Battery charging power (kW).
P_{dch}	Battery discharging power (kW).
P_g	Power purchased from grid (kW).
P_{hl}	Power usage of base load (kW).
P_{HP}	Power consumption of HP (kW).
R_{in}	Thermal resistance between building and ambient (°C/W).
R_{io}	Thermal resistance between building and thermal mass (°C/W).
C_l	Thermal capacity of the thermal mass (J/°C).
C_{in}	Thermal capacity of the building (J/°C).
λ	Solar radiation absorption factor.
P_{PV}	PV output Power (kW).
SOC_0	Initial SOC of BSS (%).
T_l	Building's lumped thermal mass temperature (°C).
T_o	Ambient temperature (°C).
T_{in}	Indoor temperature (°C).
T_{return}	Temperature of return water from building (°C).
T_{TSS}	Chilled/hot water temperature stored in TSS (°C).
Q_{HP}	Thermal energy generated by HP (kW).
Q_{td}	Thermal energy demand (kW).
Q_{TSS}	Thermal energy stored in TSS (kW).
Y	Planned project lifetime.
BSS	Battery storage system.
COP	Coefficient of performance.
DR	Demand response.
DRP	Demand response program.
HP	Heat pump.
HVAC	Heating, ventilating, and air conditioning.
MPC	Model predictive control.
OBTS	Optimal BSS and TSS sizing.
PSO	Particle swarm optimization.
RES	Renewable energy resources.
RTP	Real-time pricing.
SBEMS	Smart building energy management system.
SOC	Battery state of charge.
TOU	Time-of-use.
TSS	Thermal storage system.
LCC	Life cycle cost.

1. Introduction

Worldwide, the installed capacity of photovoltaics (PVs) has significantly increased in recent years. The PV system is one of the top-ranked renewable resources in many countries including USA, China, Japan, India, and Australia. In 2017, the global installed (on-grid and off-grid) PV capacity reached 98 GW which was nearly one-third of the total 402 GW load [1]. However, the renewable energy buyback rate is expected to significantly drop in the near future. This buyback price reduction is due to power system challenges, such as frequency regulation, reverse power and voltage imbalance issues which are caused by high

PV penetration. A potential solution that may be beneficial for both end-users and utilities is to increase PV self-consumption. This can be efficiently achieved using energy storage systems and residential flexible loads such as heat pumps (HPs) and electric vehicles (EVs) [2, 3]. Energy storage systems are frequently being applied to minimize various issues of RES-penetrated power networks. A comprehensive review of various energy storage systems is presented in [4].

Accordingly, residential customers can reduce their electricity costs by capitalizing their dispatched power. This can be done by i) optimizing the capacities of renewable energy resources (RESs) and energy storage systems, ii) utilizing HPs and heating, ventilation, and air conditioning (HVAC) systems coupled with thermal energy storage systems and, iii) implementing demand response programs (DRPs) to spread the HP load throughout the day based on electricity price tariffs and the availability of RESs [5, 6]. In Australia, residential end-users have moved to install rooftop PV systems to reduce electricity bills. However, they still have to pay for electricity due to high electricity prices during peak-load hours when PV production is not sufficient. A practical solution is to implement demand response programs, flexible loads, and energy storage systems to take full advantage of PV power production.

Electrical storage systems (e.g., Lead-acid and Li-ion batteries) have limitations including short lifespan, limited number of cycles, and high initial cost that make them unaffordable for most applications [7, 8]. Comparatively, thermal storage systems (TSSs) [4] and pumped-hydro storage systems [8, 9] are eco-friendly options that can provide more sustainable solutions. More importantly, TSSs make HVAC systems flexible with suitable responses to time-varying electricity prices. Hence, a combination of TSSs and electrical storage systems could provide a more economical and eco-friendly solution compared to utilization of only electrical storage systems. Therefore, the motivation of this study is to provide a low-cost solution to end-users with a low environmental impact using TSSs and battery storage systems (BSSs) for energy management applications.

Many researchers have focused on finding optimal component sizes of RES and storage systems for smart buildings. Some papers have applied flat electricity tariffs or average load as input data to find optimal sizes of RESs and electrical energy storage [1, 1]. Most publications rely on simple charging algorithms [1, 1]. Recent research has considered optimal battery charging and discharging in their sizing strategies. However, the effect of flexible loads such as HPs and HVAC systems on RES and BSS sizes as well as PV self-consumption have not been investigated.

In [1], a stochastic approach based on a Monte Carlo simulation (MCS) and particle swarm optimization (PSO) was proposed for sizing a smart household energy system, taking into account the demand uncertainty. A convex programming method for finding optimal size and control of energy in smart homes, with PV generation and battery storage has been introduced in [1]. This structure is employed for three different buildings in California and Texas. The optimal size and control are investigated over several time horizons, considering maximum power exportation to the grid, BSS cost, and load demand patterns. In [1], the authors used a mixed integer nonlinear programming method to perform optimal size and operation of the battery storage system for a smart home. In [1], mixed-integer linear

programming (MILP) was implemented to find the optimal battery and PV sizes for a determined location considering both demand and time-of-use (TOU) tariff. Another MILP was also applied to optimally schedule the PV-battery system, with the aim of reducing electricity bills. However, the effect of flexible loads such as HPs and HVAC systems on RES and BSS sizes were not considered in the aforementioned studies.

In [1], a MILP framework was applied to quantify the required battery capacity. However, the solution depends on different DR-based load patterns. The sizing and analysis of renewable energy and BSSs were introduced in [1]. A hybrid model was proposed using MILP to maximize the use of renewable energy and reduce load demand on the grid. Weather prediction was used to determine the optimal size of the wind turbine as well as the thermal load and PV profiles for a residential building. The aforementioned literature presents useful backgrounds; however, the effect of thermal energy storage sizing on battery size in smart buildings has not been considered in these publications.

The effects of different electricity pricing tariffs on PV and electrical energy storage systems are investigated in [2]. In their work, the profitability and sizing of a PV system with a battery are analyzed from an economic perspective for residential buildings. However, the effect of DRPs is not considered in the sizing of components. The authors [2] have developed a MILP model for the optimal sizing and operation of HP based building energy systems. Their analysis demonstrated that the size of the HP is slightly affected by the scenario assumptions, while the optimal sizing of PV significantly depends on load profiles. However, the effect of flexible HP coupled with TSS on the dimension of BSS has not been considered. A MILP algorithm is introduced in [2]. This algorithm is presented to find the optimal size and operation of electric boiler and thermal storage in combination with a PV system. A considerable storage size was only obtained during the large fluctuation in electricity prices or by using the large PV size. The authors [2] investigate the parameters that affect the optimal size of BSS for grid-connected PV systems. The subject was to improve the self-consumption of PV systems by determining the battery size based on electricity tariffs, and battery performance and price. The battery size was largely affected by feed-in electricity price. Similarly, the pricing structure is applied to find the optimal size of PV and BSS systems of a smart house in [2].

Boeckl et al., [2] have presented a technical consideration sizing method to design PV and battery systems for different households. This paper considers different household load profiles based on a behavior model and life patterns of different end-users in a stochastic method. However, considering DR is crucial to design a PV battery system which has been ignored in aforementioned paper. Another work [2] presented an analytical strategy for sizing battery storage based on minimizing energy cost for a battery storage owner. This paper developed a simple analytical method to size battery for peak-load shaving. However, DRPs are already practical by developing smart meters. Therefore, controlling HVAC systems as the devices that consume the most power in residential buildings is important to consider for designing a battery. The sizing of rooftop PV systems with HPs and BSS with the focus on changing economics and regulatory is evaluated in [2]. In [2], the authors presented an optimization model to investigate the effect of HPs on the size of a PV system with BSS. The results showed that HPs as shiftable loads are required to avoid under-sizing of

PV systems. However, the effect of HPs coupled with TSS on BSS size has been ignored. An interesting research on electrical and heating components sizing is presented in [2]. The authors have applied forecast-based operation approaches for PV-battery and power-to-heat systems to improve economics of the house. The results show reduction in levelized costs of electricity compared to a self-consumption maximizing strategy. In [3], the authors have investigated the effects of thermal and electrical loads, TSS, EV, and power sharing among neighbors on PV system sizing for residential buildings. A genetic algorithm is adapted to optimize: i) the quantity of PV capacity installed on each facade of the building, and ii) the size of electric storage to increase PV self-consumption when the system is profitable. An optimization design strategy is provided in [3] for implementing building-integrated PV with electricity storage in the early conceptual and preliminary design process of a building. The method optimizes the size and positions of the PV panels and size of the BSS to enhance the net present value of the whole system during the project lifetime. However, the effects of load management and thermal storage have not been considered to attain high PV self-consumption rates. Furthermore, the impacts of HP load management on the capacity design of TSS and BSS are not included in the aforementioned studies.

Accordingly, there is a research gap in developing effective sizing strategies for HPs coupled with TSS to respond to DRP while minimizing life cycle cost. Therefore, the key goals of this paper are to first find the optimal sizes of TSS and BSS based on TOU tariff to increase PV self-consumption. Then, after determining the optimal BSS and TSS sizes, developing a smart management strategy to decrease the electricity cost of residential buildings is next goal of this paper. The well-known heuristic PSO approach is applied for optimal thermal and electrical storage component sizing. MCS is implemented to generate a set of random inputs using their probability density functions. After determining optimal BSS and TSS sizes, MPC is applied for real-time optimal operation of smart buildings.

The contributions of this study can be summarized as follows:

- A new optimal BSS and TSS sizing (OBTS) solution is proposed for thermal and electrical storage systems to minimize annual electricity costs of smart buildings with rooftop PVs while minimizing life cycle cost. Optimal BSS and TSS charging and discharging are key elements of the proposed OBTS that is considered in the optimal sizing. These elements have not been widely considered together by other researchers for optimal TSS and BSS sizing studies. Furthermore, cost comparison for various case studies is presented.
- A control scheme is developed for real-time smart building energy management system (SBEMS) to increase PV self-consumption and reduce electricity costs. The real-time charging and discharging of BSS and TSS are achieved by using the proposed SBEMS based on RTP.
- The proposed SBEMS is validated experimentally in a real-time environment using facilities available in the Smart Energy Laboratory at Edith Cowan University, Australia. Furthermore, different sizes of BSS and TSS are applied to verify the results of proposed OBTS.

The remaining part of this paper is divided into six sections. Section 2 describes the system

model. The proposed OBTS and SBEMS are introduced in Section 3. Simulation results and experimental verifications are presented in Sections 4 and 5, followed by conclusions in Section 6.

2. System Model

In this paper, MCS is implemented in the proposed optimal BSS and TSS sizing (OBTS) strategy, to consider uncertainties associated with weather data such as solar radiation and ambient temperature. The uncertainties in weather prediction are described in MCS by proper probability distribution functions (PDFs). The one-year weather data record is used as the input data for MCS. The daily inputs with 10-min discrete time steps for optimization are then generated based on the daily recorded data. These data sets are sent to PV and building thermal models, to predict PV production and the thermal load profile of residential buildings. Then, the system model is described in two parts, the electrical system model and the thermal system model.

2.1. Electrical System Model

2.1.1. Battery Model

Battery models are mainly determined by their charging and discharging limitations. The stored energy in battery for each time step can be calculated as:

$$E_{t+1}^{batt} = E_t^{batt} + P_{ch,t}\eta_{ch} - \frac{P_{dch,t}}{\eta_{dch}} \tag{1}$$

where η_{ch} and η_{dch} represent the efficiency during charging and discharging modes, respectively. Then, the battery state of charge (SOC) can be expressed as:

$$SOC_{t+1} = \frac{E_{t+1}^{batt}}{E_{max}^{batt}} \times 100 \tag{2}$$

$$SOC_{min} < SOC_t < SOC_{max} \tag{3}$$

where E_{max}^{batt} is the maximum stored energy (kWh). An additional constraint is added to avoid that the charging and discharging occur simultaneously:

$$P_{ch,t} \cdot P_{dch,t} = 0 \tag{4}$$

The depth of discharge (DOD) is modeled by [3]:

$$E_t^{batt} \geq C_{batt}(1 - DOD) \tag{5}$$

where C_{batt} represents the size of BSS.

2.1.2. PV Model

The PV output power is calculated based on the solar irradiation data (I_s) [3].

$$P_{\mathrm{PV},t} = I_{s,t} A_{\mathrm{PV}} N_{\mathrm{PV}} \eta_{\mathrm{PV}} (1 - 0.005(T_{o,t} - 25)) \tag{6}$$

where A_{PV} and N_{PV} represent the area and number of PV module, respectively. η_{PV} represents the efficiency of PV system.

2.1.3. Electric Load Model

Electrical loads can be incorporated with the base and HP loads as shiftable loads. In this paper: i) the household appliances such as lighting, refrigerators, freezers, ovens, stoves and computers are considered as the base loads, ii) the input data for generating daily load profile by MCS is provided in [3] and, iii) the SELAB building at Edith Cowan University in Western Australia with an average daily power consumption of 18 kWh is selected as the residential building.

2.2. Thermal System Model

In most buildings, air conditioners, radiators and fan coil units are employed to regulate room temperature by using thermostats. The state of the on/off relay can be determined by the hysteresis control rule in cooling mode as follow [3]:

$$\mathbb{U}_{t+1} = \begin{cases} 0 & \text{if } T_{in,t} \leq \underline{T}_{in} \\ 1 & \text{if } T_{in,t} \geq \overline{T}_{in} \\ \mathbb{U}_t & \text{otherwise,} \end{cases} \tag{7}$$

where T_{in} is the indoor temperature which is function of outdoor temperature, solar radiation, internal heat gain, and building thermal mass. $\overline{T}_{in}$ and $\underline{T}_{in}$ are upper and lower boundaries of temperature set-point. $\mathbb{U}$ is the discrete state of the relay which switches the heat distributor on and off; according to the hysteresis control rule.

The Smart Energy laboratory (SELAB) building is modeled by the heat dynamic state-space model of [3] and [3]:

$$\begin{bmatrix} \dot{T}_l \\ \dot{T}_{in} \end{bmatrix} = \begin{bmatrix} -\frac{1}{R_{in}C_l} & \frac{1}{R_{in}C_l} \\ \frac{1}{R_{in}C_{in}} & -(\frac{1}{R_{io}C_{in}} + \frac{1}{R_{in}C_{in}}) \end{bmatrix} \begin{bmatrix} T_l \\ T_{in} \end{bmatrix} + \begin{bmatrix} 0 \\ \frac{1}{C_{in}} \end{bmatrix} \mathbb{U}\dot{Q}_{td} + \begin{bmatrix} 0 & 0 & 0 \\ \frac{1}{R_{io}C_{in}} & \frac{\lambda}{C_{in}} & \frac{1}{C_{in}} \end{bmatrix} \begin{bmatrix} T_o \\ I_s \\ I_g \end{bmatrix} \tag{8}$$

where ideally $T_{TSS} = T_{HP}$, thus, $\dot{Q}_{td} = \dot{m}_{td}c_p(T_{TSS} - T_{return})$. The model parameters are identified utilizing a nonlinear regression algorithm by measuring T_{in}, T_o, I_s, I_g, and Q_{td} [5]. The building model is presented and validated in [5].

The daily thermal demand is calculated based on the building model of equation 8. In each time step, the updated indoor temperature ($\dot{T}_{in}$) and building lumped thermal mass temperature ($\dot{T}_l$) are calculated based on the present temperatures, solar radiation, outdoor temperature, and the heat gain. The calculated temperatures (equation 7) are used to determine the ON/OFF state of the heat distributor switch. When the heat distributor is ON, the required thermal energy is assumed to be $\dot{Q}_{td}$.

2.2.1. Heat Pump Model

The heating/cooling capacity of an HP ($\dot{Q}_{HP}$) can be calculated based on the flow rates and temperatures of water inlet and outlet of HP as well as the coefficient of performance

(COP) [3].

$$\dot{Q}_{HP} = \dot{m}_{HP} c_p (T_{HP} - T_{return}), \quad \text{COP} = \frac{\dot{Q}_{HP}}{P_{HP}} \tag{9}$$

The heat transfer of the HP is presented in A, in detail. In this paper, a minimum runtime of 10 minutes is considered for HP and the installed HP at the SELAB building is considered for the proposed model. The HP is a ground source heat pump. Details of the HP are presented in A.

2.2.2. Thermal Storage System (TSS) Model

TSS is modeled based on the stratified two-layer tank. Fig. 1 shows the scheme of thermal system in cooling mode. As the TSS is involved to the closed-loop system, the sum of the volume of return water (m_{return}) and chilled/hot water (m_{TSS}) is always constant and equal to the volume of TSS (m_{tot}):

$$m_{tot} = m_{TSS} + m_{return} \tag{10}$$

The dynamics of TSS system can be expressed by the change in volume (m_{TSS}) and temperature of the chilled/hot water layer of TSS (T_{TSS}). This model can be simplified by neglecting losses to the surrounding area. Therefore, based on the heat and mass flow balance concept, the TSS model can be described by the following first-order non-linear differential equation [5]:

$$\frac{\mathrm{d}m_{TSS}}{\mathrm{d}t} = \dot{m}_{HP} - \dot{m}_{td} \tag{11}$$

$$\frac{\mathrm{d}Q_{TSS}}{\mathrm{d}t}(m_{TSS},T_{TSS}) = Q_{TSS}^{\text{in}} - Q_{TSS}^{\text{out}} = \dot{m}_{HP} c_p T_{HP} - \dot{m}_{td} c_p T_{td} \tag{12}$$

On the other hand, the product rule derivative of equation (12) is given by:

$$\frac{\mathrm{d}Q_{TSS}}{\mathrm{d}t}(m_{TSS},T_{TSS}) = c_p\left(\frac{\mathrm{d}m_{TSS}}{\mathrm{d}t} \cdot T_{TSS} + m_{TSS} \cdot \frac{\mathrm{d}T_{TSS}}{\mathrm{d}t}\right) \tag{13}$$

In charging mode ($\dot{m}_{HP} > \dot{m}_{td}$), a constant mass water flow rate is considered which is $\dot{m}_{HP} > \dot{m}_{td}$. Consequently, TSS is always charged and $T_{td} = T_{HP}$ since the HP is operating. Therefore, the following equation can be derived from Eqs. (12) and (13):

$$\frac{\mathrm{d}m_{TSS}}{\mathrm{d}t} \cdot T_{TSS} + m_{TSS} \cdot \frac{\mathrm{d}T_{TSS}}{\mathrm{d}t} = (\dot{m}_{HP} - \dot{m}_{td}) T_{HP} \tag{14}$$

Subsequently, the derivative of temperature of the bottom layer water at each time step can be expressed by substituting Eq. (11) into (14):

$$\frac{\mathrm{d}T_{TSS}}{\mathrm{d}t} = \frac{(\dot{m}_{HP} - \dot{m}_{td})(T_{HP} - T_{TSS})}{m_{TSS}} \tag{15}$$

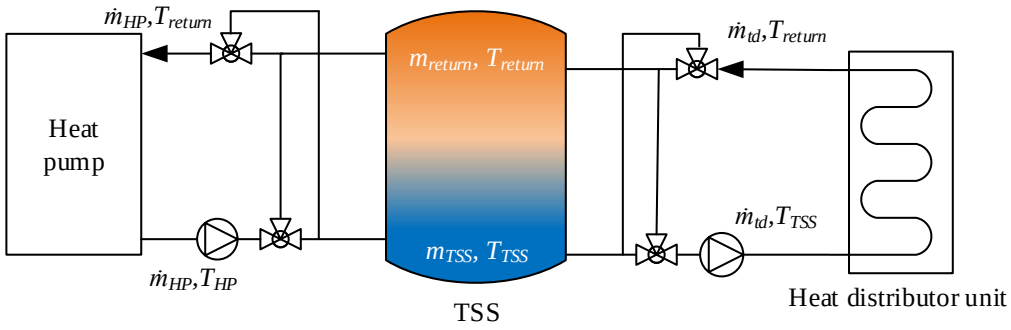

Figure 1: Scheme of thermal system (in cooling mode).

3. Formulation of the optimum design problem

The system model presented in Section 2 is used to formulate and implement the proposed OBTS and SBEMS.

The aim of this work is to design an optimal model for a smart home. This model encompasses rooftop PV, battery and HP system coupled with TSS. The sizes of battery and thermal storage tank are optimized considering the cost associated with initial investment of each component, operation, maintenance, equipment replacement, and electricity purchase. Then, the proposed SBEMS is employed to real-time manage the physical system composed of the smart building based on the optimal sizes of TSS and BSS.

3.1. Formulation of Proposed OBTS

OBTS is presented with inner and main optimization loops. These two loops are described in Sections 3.1.1 and 3.1.2.

3.1.1. Inner Optimization Loop

Inner optimization loop is proposed here to manage the thermal energy system, thus minimizing operation costs, while controlling building temperature within thermal comfort zone. The inner loop is also used to control the battery charging/discharging to enhance the integration of the PV system with loads based on TOU tariff.

During the peak and flat periods, the battery is charged by the surplus PV output power. Besides, the charging can also be performed over the night period to store enough energy. The load is supposed to cover first by the PV system when it has a sufficient output power. While the redundant power is used to charge the battery, or it can be sent to the utility grid. Conversely, the battery is discharged when the PV power is not enough to meet the load. The discharging continues until the minimum level of the SOC. Meanwhile, the power shortage is covered by purchasing power from the grid.

The objective function is used to minimize electricity costs with the aim of the most effective utilization of PV generation. In this study, the objective function is expressed as

follows:

$$\min \quad \sum_{m} C_{g,m} \tag{16}$$

where

$$C_{g,m} = C_m \cdot P_{g,m} \tag{17}$$

Equation (16) is subject to:

$$m_{TSS}^{min} \leq m_{TSS} \leq m_{TSS}^{max} \tag{18}$$

$$P_{g,m} + P_{PV,m} + P_{dch,m} - P_{ch,m} - P_{HP,m} - P_{hl,m} = 0 \tag{19}$$

$$Q_{HP,m} - Q_{TSS,m} - Q_{td,m} = 0 \tag{20}$$

where C_m is the time-of-use electricity pricing tariff ($\$/kWh$) as described in Table 1 [3]. $Q_{TSS,m}$ represents the charging mode of TSS. The stored thermal energy is consumed on the same day and m_{TSS} reaches the initial stored thermal energy $m_{TSS,0}$ at the end of day. Note that the TSS model is simplified to reduce the complexity of solution. In proposed OBTS, it is assumed the HP generates chilled/hot water at the required temperature. Therefore, TSS is modeled based on inlet and outlet water of TSS based on equation (11).

Table 1: Time-of-use electricity pricing tariff for Western Australia.

Time of day	Price ($)
7am-3pm	0.287
3pm-9pm	0.548
9pm-7am	0.151

3.1.2. Main Optimization Loop

The main optimization loop is incorporated to investigate the effect of the PV self-consumption system on BSS and TSS sizes for residential buildings. Accordingly, BSS and TSS sizes are determined by the end of this loop. The objective function of this loop is proposed to calculate the LCC of the system. Thus, optimal sizes are determined for minimum cost. The objective function of this loop is:

$$\min \quad \sum LCC \tag{21}$$

where

$$LCC = CC_{TSS} + CC_{BSS} + \sum_{y=1}^{Y} \frac{MC_{TSS} + MC_{BSS} + RC_{BSS} + (1+i)^y \sum_{d=1}^{365} C_{g,d}}{(1+l)^y} \tag{22}$$

In equation (LCC), y is the year of operation of the system, Y is the planned project lifetime, i is the expected annual energy price increase (inflation) during the project lifetime, and l is discount rate.

Table 2: Number of full cycles based on depth of discharge [4].

DOD	10	20	30	40	50	60	70	80	90	100
N_{tot}	43000	35000	27500	20000	15000	10000	6250	3200	2700	2600

3.1.3. Constraints of Main Optimization Loop

Limitation of BSS and TSS. A fixed typical rooftop PV size of 5 kWp is used in this work. The limitations of BSS and TSS depend on the physical parameters of the residential building. Therefore, the battery and TSS are used as follows:

$$0 \leq m_{TSS} \leq 3000\ L \tag{23}$$

$$0 \leq C_{batt} \leq 10\ kWh \tag{24}$$

Life Cycle Cost of Thermal Storage System. The number of on/off HP cycles reduces for higher TSS volumes. However, when the capacity of the tank is increased, the tank thermal losses and the initial capital cost will also increase. Therefore, the thermal losses of tank are compensated by energy-saving caused by the reduction of HP cycling losses. On the other hand, the stored chilled/hot water in TSS is produced and consumed on the same day. This constraint is to minimize thermal losses of TSS. Hence, the life cycle cost of TSS is determined by the initial capital cost (CC_{TSS}) and the maintenance cost (MC_{TSS}). The minimum lifetime of a water storage tank is 25 years. Therefore, the replacement cost of TSS is not considered in this work.

Life Cycle Cost of Battery Storage System. The charging and discharging cycles of the BSS is usually reduced due to battery degradation. The rate of this degradation largely depends on battery (calendar and cycle) aging, as well as the current state of life [4]. Therefore, the age of the battery is mainly determined by the number of cycles and time. The expected number of cycles (before the end of battery life) is often mentioned by manufacturers. The rain-flow-counting method is used to determine the number of cycles and subsequently the lifetime of BSS. The lifetime of the battery based on DOD is described by [4]:

$$L_{BSS} = \sum_{DOD=0.1}^{DOD=0.8} \frac{N_{cyc}(DOD)}{N_{tot}(DOD)} \tag{25}$$

where N_{cyc} is the number of full cycles in the specified DOD, and N_{tot} is the maximum number of full cycles based on DOD. The end of battery life with different DOD cycles is when $L_{BSS} = 1$. Table 2 shows the number of full cycles N_{tot} versus DOD [4].

This work considers battery degradation costs within the operational and maintenance costs (MC_{BSS}). A replacement cost of battery (RC_{BSS}) should be considered in addition to battery operation and maintenance costs. Table 3 shows the costs associated with initial capital costs of BSS (CC_{BSS}) and TSS, as well as replacement and maintenance costs. CC_{BSS} represents the capital cost associated with the battery and its inverter.

Table 3: Costs associated with BSS and TSS.

CC_{TSS}	MC_{TSS}	CC_{BSS}[4]	RC_{BSS}	MC_{BSS}
100 \$/100L	1 \$/100L	850 \$/kWh	850 \$/kWh	2% of CC_{BSS}

3.1.4. Proposed Optimization Approach

Fig. 2 shows the proposed OBTS structure. The PSO algorithm is used as the main optimization tool to minimize the LCC of the system. This heuristic approach is applied to simultaneously determine the BSS and TSS sizes while optimizing the operations of battery and HP. Integer variables such as HP on-off cannot be included in the convex optimization problem. PSO is a well developed technique to deal with nonlinear and nonconvex constrained problems to find global optima [4]. PSO is a promising tool that does not require the computation of derivatives. Therefore, PSO is applied in the inner loop to optimize HP on-off and battery charging and discharging. In main optimization loop, PSO creates a random population of possible solutions named particles. Each particle consists of the random sizes of BSS and TSS. In each iteration, particles are sent to the inner optimization loop. The objective of inner loop is to minimize the daily electricity cost and maximizes the PV self-consumption. The annual electricity cost is then evaluated for each particle. Particles then move toward global and local solutions by evaluating LCC. Consequently, the optimal sizes of TSS and BSS are determined by minimizing LCC.

3.2. Formulation of Real-time Optimal Operation

The proposed SBEMS is employed to manage the physical system composed of the smart building based on the optimal sizes of TSS and BSS. The building is equipped with PV panels and BSS and connected to the grid. Total electrical base load is supplied by PV, BSS, and the grid. While the thermal load is supposed to be supplied by the HP coupled with TSS. In general, the daily HP input and electrical load can be met by the grid, PV panels, and batteries. The objective is to propose an SBEMS that can achieve minimum electricity cost and maximum PV self-consumption. The main advantage of the proposed SBEMS is the possibility to simultaneously control the BSS and HP coupled with TSS. After determining the optimal BSS and TSS sizes, MPC is used for the real-time optimal operation of the smart building. The schematic diagram of the proposed SBEMS is shown in Fig. 3. MPC uses the system model to predict the future evolution of the smart building and perform real-time control actions [4]. The main objective of using MPC is to control the HP (on/off), in order to shift HP load based on the DRP, by producing sufficient chilled/hot water. Moreover, this controller is responsible to manage the charging and discharging of BSS. The cost function for the MPC based on RTP tariffs is a trade-off between the minimum cost of the total daily electricity and PV power exportation to the grid. At the same time, producing enough chilled/hot water which is subject to the dynamic constraints as follows:

$$\min_{u_k} \quad \sum_{j=k}^{k+N-1} C_g(j|k) \tag{26}$$

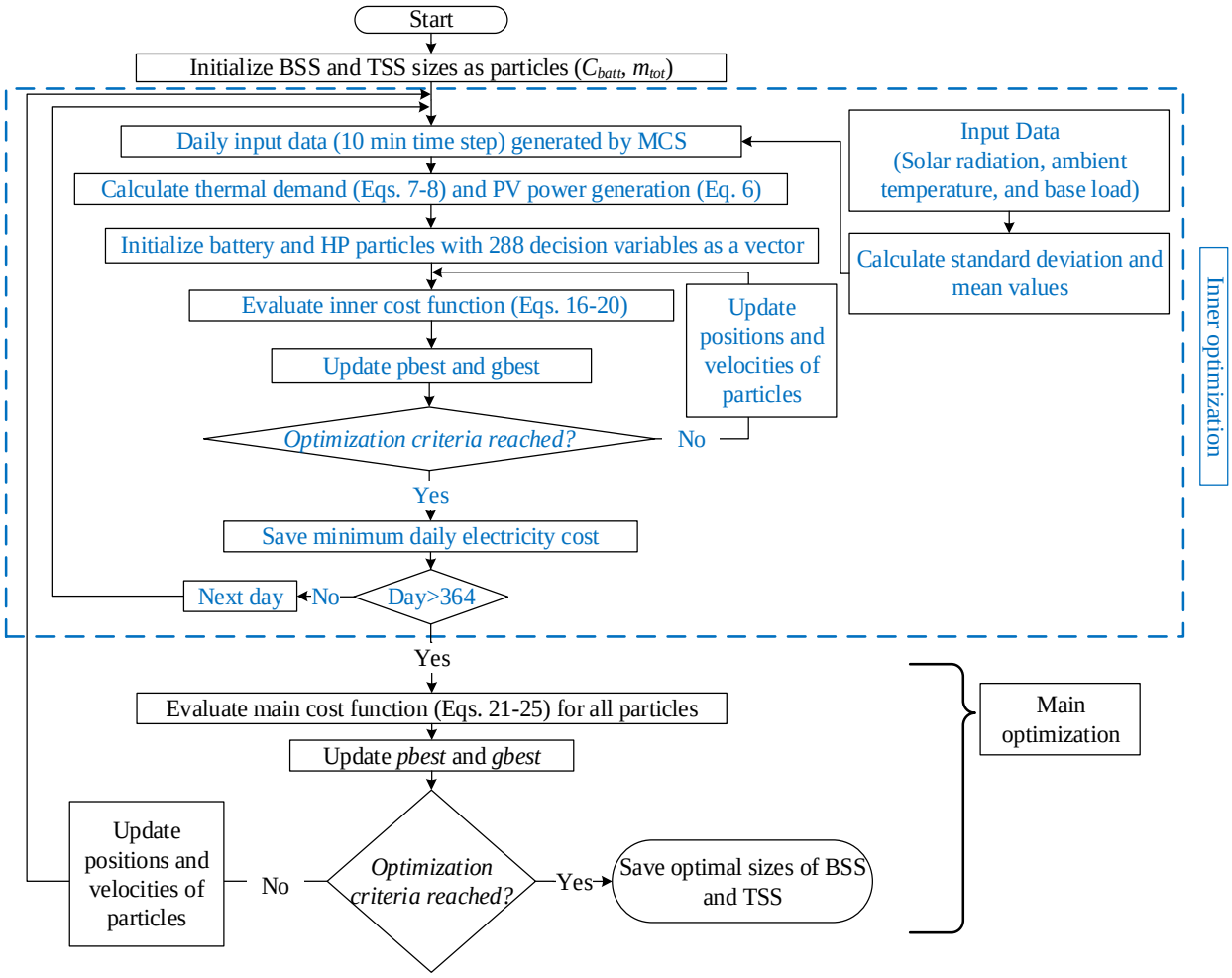

Figure 2: Flowchart of proposed OBTS.

subject to

$$x(j+1|k) = f(x(j|k), u(j|k), d(j|k)), \quad \forall j = k, k+1, \ldots, k+N-1 \tag{27}$$

$$y(j|k) = g(x(j|k), u(j|k), d(j|k)), \quad \forall j = k, k+1, \ldots, k+N \tag{28}$$

where N is the prediction horizon, u is the binary decision variable, x is the state variable which represents T_{in}, m_{TSS} and SOC, y is the output which represents P_g, and d is the disturbance. The model-based optimization problem is solved over a finite horizon. The horizon prediction is $N = 24$ hours. The control sampling time is 5 minutes. The prediction horizon is considered equal to the control horizon. In this paper, the MPC optimization problem is defined as the problem of finding an optimal reference power for the heat pump and a discharge/charge reference power for BSS to supply the load. This can be described as follows: The electrical system dynamic equations (1)-(6) and the thermal system dynamic equations (7)-(15) are the main dynamics of the MPC while equations (19)-(20) and Table

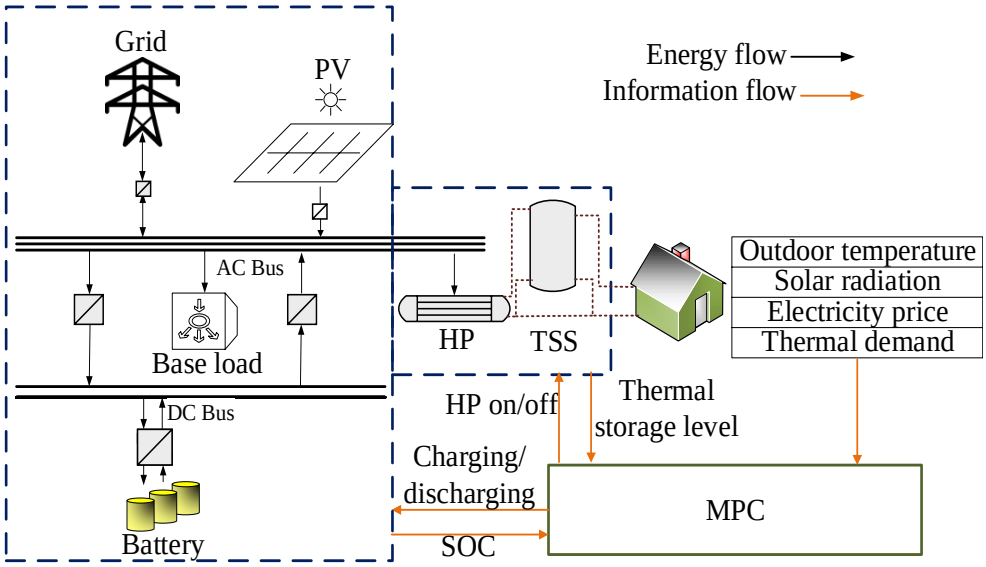

Figure 3: Schematic of energy management system.

4 correspond to the constraints of the system. Figure 4 presents an overview of the MPC is implemented in the proposed SBEMS. An optimal control problem is formulated and solved in each time step to obtain the control signal. The formulation is based on the current system conditions, a prediction of external influences and the future system state. A model of the system is used to evaluate the impacts of the controls on the state of the system and to compute the optimal control solution. The first part of the computed solution is applied to the system. The procedure continues to find a control trajectory of u that minimizes the cost function (26).

4. Simulation Study of Proposed OBTS

In this paper, the SELAB building is considered as a residential building with an average of 18 kWh daily power consumption in Western Australia. This building is equipped with a 5-kWp rooftop PV system and a 10-kW water source HP system for space heating and cooling. The project liftime is assumed to be 25 years. The simulations are performed with operating constraints as presented in Table 4. The percentages of m_{TSS} are associated with the volume of TSS (m_{tot}). In the grid-side, it is preferred for the renewable output power to be consumed locally, to avoid the risk of causing rapid ramp generation on the conventional generators. Furthermore, selling power price rates are appealing; therefore, the revenue of selling PV power to the grid is not considered in this study. The main objective of OBTS is to find optimal sizes of thermal and electrical systems, with the aim of decreasing LCC and increasing PV self-consumption. Detailed simulations are performed for four cases.

4.1. Case I: Base Case

In this case, the SELAB building is simulated without BSS and TSS. The reason for this is to use this base case results to evaluate and analyze other scenarios. Fig. 5 shows the average hourly power consumption for four seasons. The base load and HP load are without

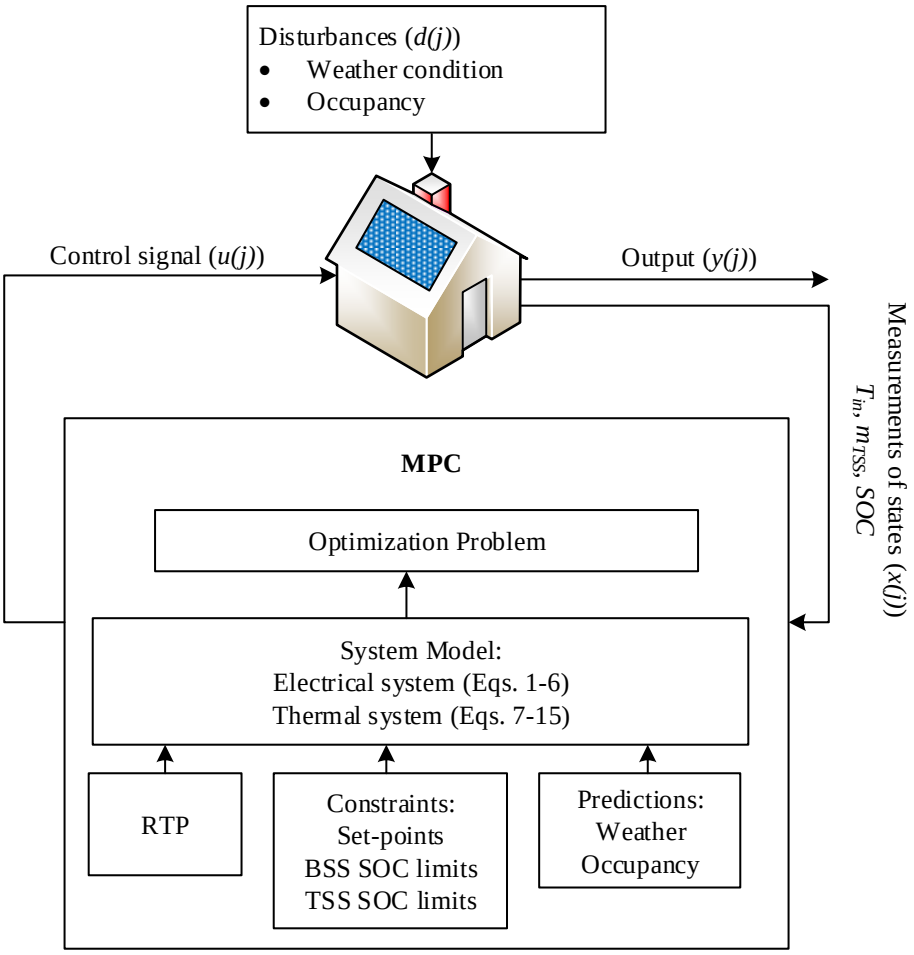

Figure 4: Flowchart of the MPC procedure.

Table 4: Operating constraints used in simulations.

SOC_0	SOC_{min}	SOC_{max}	m_{TSS}^{min}	m_{TSS}^{max}	$m_{TSS,0}$
50%	10%	90%	5%	100%	5%

any storage systems. The thermostatic control is utilized to determine the HP on-off signal, thus to supply the thermal load. The demand is increased in the peak-load period due to HP operation, in particular in summer and winter seasons.

4.2. Case II: TSS Only

The HP system is employed with a TSS. The optimal size/volume of TSS (determined by the proposed strategy of Section III) is 2000 liters. The life cycle cost of TSS is considered in this scenario. The HP system operates without an initial stored thermal energy in TSS, at first time step in each day. In order to avoid TSS thermal losses, it is assumed that: i) the TSS is covered with 100 mm insulation layer, and ii) the OBTS algorithm keeps the TSS without stored chilled/hot water at the end of the day. Fig. 6 shows the base load and

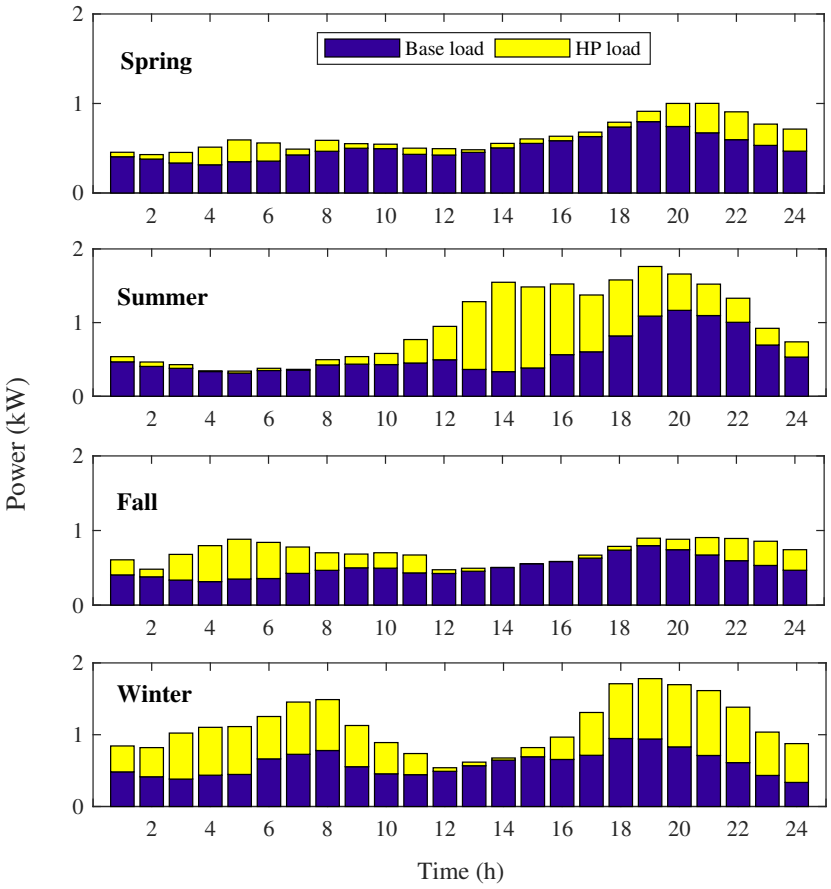

Figure 5: Case I: Average hourly power consumption for four seasons.

the shifted HP load by the OBTS algorithm for four seasons. The results show that most of the HP load is shifted from peak-load hours (6pm-9pm) to periods with PV generation or the periods with lower electricity prices.

4.3. Case III: BSS Only

The building is simulated with BSS and HP systems without any TSS. The optimal size of BSS, considering the operating and economic constraints indicated in Table 5, is 6.5 kWh. It is assumed the initial SOC is 50%. The SOC of the battery is also considered to be equal to the initial SOC at the end of each day. The HP system is considered as nonshiftable load due to the lack of TSS. A possible economic solution for cases without significant load flexibility is to store PV generation in the BSS. However, this requires a larger battery size which can subsequently raise capital cost and consequently, total life cycle cost. Fig. 7 shows the simulation results of the average hourly power dispatch for four seasons. Note that the grid power is purchased in low electricity tariff rates. However, in summer and winter, BSS is unable to fully supply the total load during the peak-load period; consequently, some power is imported from the grid.

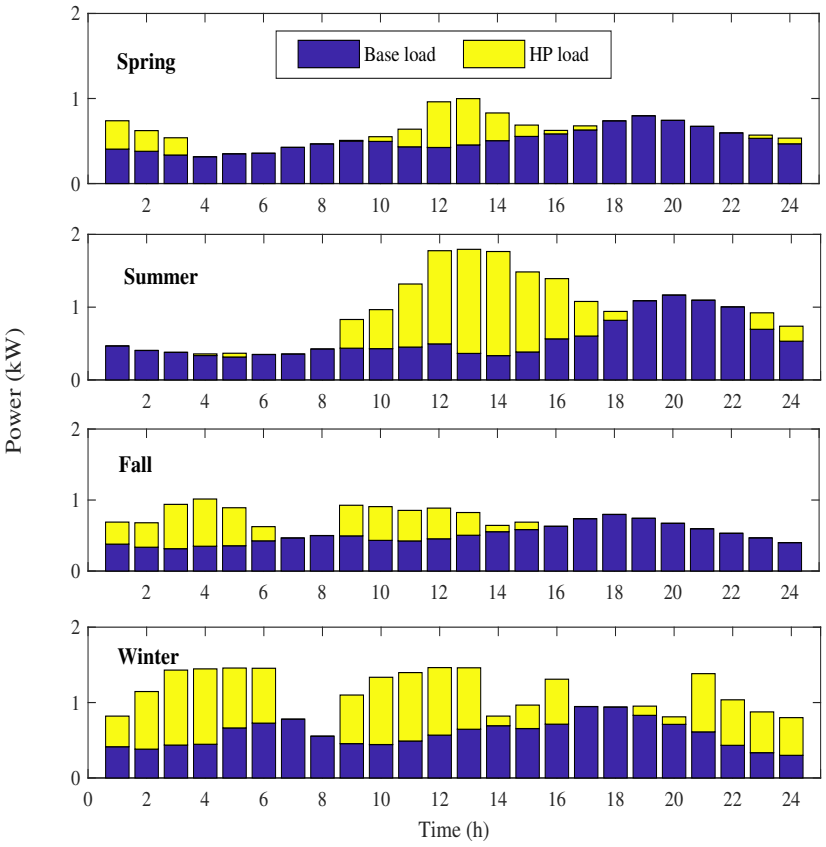

Figure 6: Case II: Average hourly power consumption for four seasons ($TSS = 2000$ *liters*).

4.4. Case IV: BSS and TSS

In this case, BSS and TSS are considered to find their optimal sizes in a residential building with a 5-kWp PV system. Fig. 8 shows the average power dispatch for four seasons with optimal sizes of BSS (4.7 kWh) and TSS (1800 liters). The simulation results prove that adding TSS to the HVAC system acquires more flexibility to the system. The introduction of TSS (with optimal size of 1800 liters) positively affects the BSS by reducing the size from 6.5 kWh to 4.7 kWh. This is done by shifting the HP load from the peak-load hours to either the lower electricity tariff or the mid-day hours when PV generation is available.

4.5. Comparison of Simulation Results of Optimal Sizing

Simulation results and cost analysis of Cases I to IV are summarized and compared in Table 5. This Table shows the optimal BSS and TSS sizes, annual PV self-consumption, annual electricity cost, life cycle cost, payback period, and the percentage of return on investment (ROI). The payback period is the time that it takes an option to have the same LCC as the base case. The payback periods of Cases II, III and IV are calculated based on the initial investment divided by the annual net cash flow. ROI is the ratio of gain to investment. ROI is defined over a life cycle of the system as follows [4]:

$$ROI = \frac{Return - Investment}{Investment} = \frac{Avoided\ Cost}{Investment} - 1 \tag{29}$$

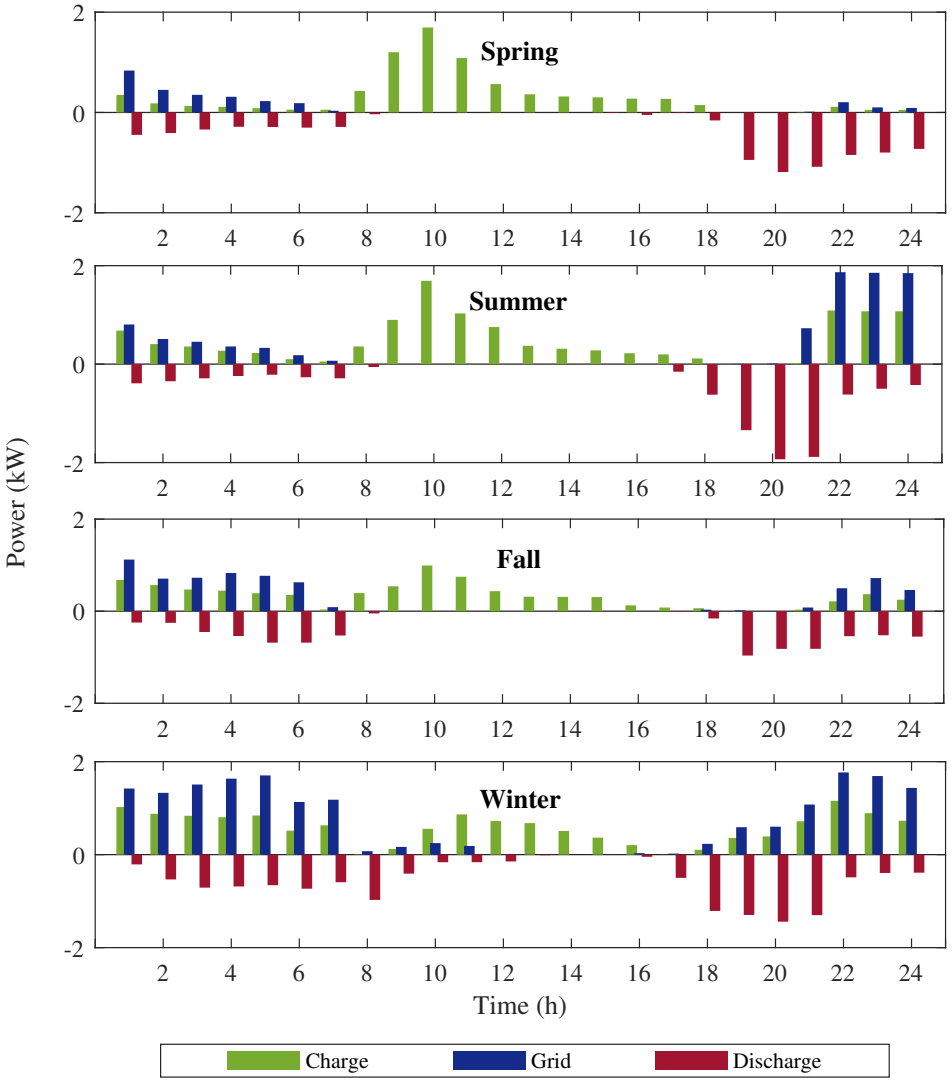

Figure 7: Case III: Average hourly power dispatch for four seasons ($BSS = 6.5\ kWh$).

However, ROI does not include the project lifetime. Thus, annualized return on investment (AROI) is necessary to amortize the full investment cost over the lifetime of the system. AROI is described as

$$AROI = [(1 + ROI)^{1/Y} - 1] \times 100\% \tag{30}$$

AROI is useful to compare the returns on Cases as investment opportunities. The total average annual PV generation is 8150 kWh. In Case I, the results show that the annual PV self-consumption is only 37.1% due to the lack of any storage systems. In this case, 62.9% of the total PV power is exported to the grid. In Case II, the introduction of TSS with the optimal volume of 2000 liters has decreased the annual electricity cost by 26.2% while PV self-consumption increased to 43.5%. As expected, this case is associated with a relatively short payback time of 5.1 years and a relatively high AROI of 6.5% over 25 years of project lifetime. In Case III, the annual electricity cost is reduced by 69.8% by adding a battery with an optimal size of 6.5 kWh to Case I; while the PV self-consumption increased to 53.3%.

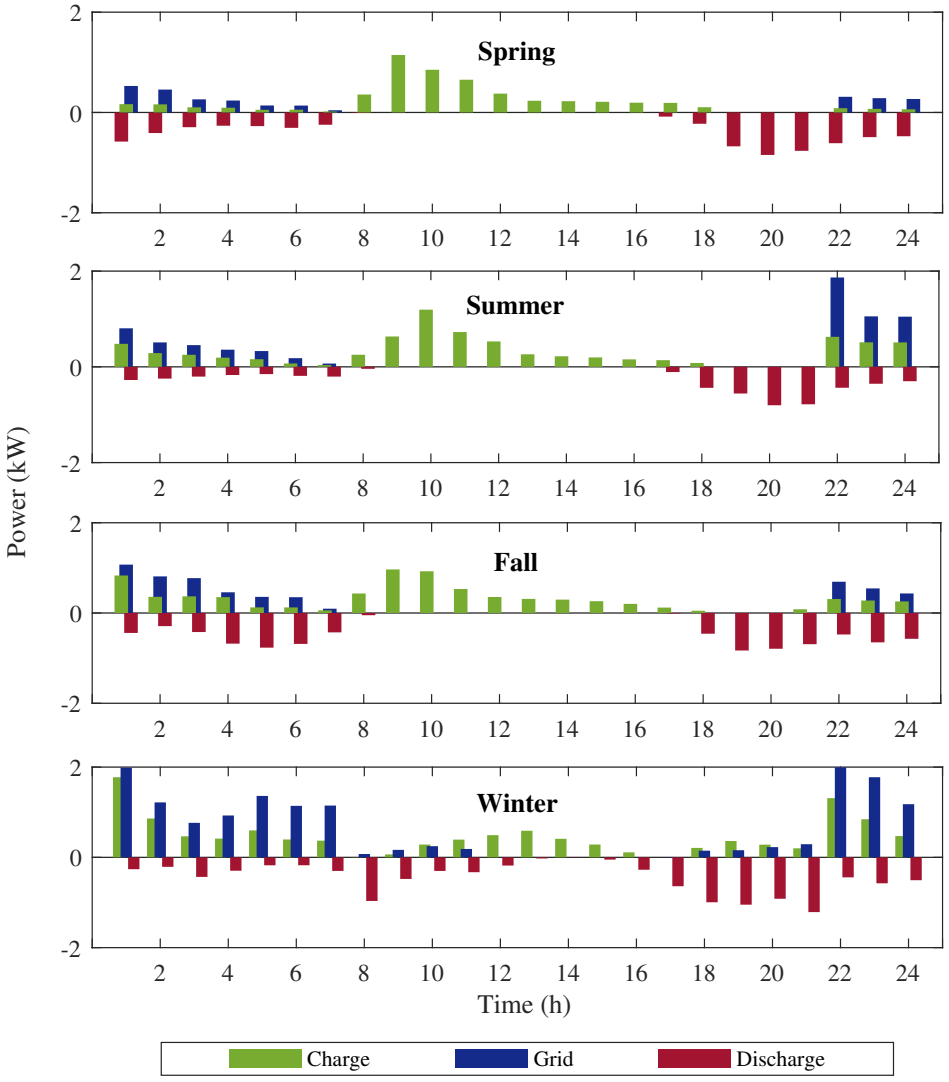

Figure 8: Case IV: Average hourly power dispatch for four seasons ($TSS = 1800$ *liters* and $BSS = 4.7$ kWh).

Moreover, LCC is improved by only 4.7% from Case II. However, the payback period and AROI are 10 years and 3.7%, respectively. In Case IV (proposed cost-effective framework of this paper), the introduction of TSS (with the new optimal volume of 1800 liters) to Case III reduces the size of BSS to 4.7 kWh. In this case, the annual electricity cost is decreased by 80.4%. Moreover, PV self-consumption is increased to 57.3%. Interestingly, the payback period is dropped to 6.8 years while the AROI is increased to 5.3%. As a result, this case has the lowest LCC in compared with other cases. Accordingly, the main advantages of using the proposed OBTS model are as follows:

- Adding the TSS in Case II with the optimal volume of 2000 liters to the residential HP system effectively increases the PV self-consumption by 17.1%, in compared with Case I. Consequently, the flexible HP system reduces annual electricity cost to $1066

Table 5: Comparison of results for Cases I-IV.

Cases	TSS size	BSS size	Annual PV self-consumption		Annual electricity cost		LCC	Payback period*	AROI**
	Liter	kWh	kWh	%	$	%	$/year	Year	%
Case I (No BSS/TSS)	-	-	3028	37.1	1445.4	-	1445.4	-	-
Case II (TSS only)	2000	-	3548	43.5	1066.4	26.2	1140.3	5.1	6.5
Case III (BSS only)	-	6.5	4351	53.3	436.2	69.8	1086	10	3.7
Case IV (BSS and TSS)	1800	4.7	4678	57.3	282.7	80.4	832.6	6.8	5.3

* Payback period is calculated based on project lifetime (25 years) and without buyback.
** Annualized return on investment.

(73.7% of Case I). The main advantage of this option is the short payback period of 5.1 years along with the higher AROI of 6.5%.

- The results of Case III show the option of adding BSS significantly reduce the electricity bill to $436.2 (30% of Case I). However, this solution may not be very attractive for some consumers due to the low return on investment (3.7%) and the long payback period (10 years).
- The proposed OBTS of Case IV reveals the significant economic impacts of introducing HP coupled with TSS to Case III. This is the most attractive solution for the consumers since the battery size is reduced by 28% (from 6.5 kWh to 4.7 kWh) and the annual electricity cost is reduced by 81% (from $1445.4 to only $282.7) with the acceptable LCC.

5. Verification of Proposed OBTS and SBEMS

5.1. Verification of Proposed OBTS

In order to verify the optimal sizing solutions of Case IV, different sizes of BSS and TSS are chosen and the corresponding costs are calculated. Sensitivity analysis results are presented and compared in Figs. 9 - 12. Fig. 9 describes simulation results for the annual electricity cost. As expected, the annual electricity cost decreases when BSS and TSS sizes are increased. However, increasing storage sizes results in higher payback period (Fig. 10) and lower AROI (Fig. 11) due to the increasing trend of capital cost. Figs. 10 and 11 show that increasing the size of BSS without adding TSS to HVAC system remarkably increases the payback period and subsequently decreases AROI. Therefore, the results of Figs. 9 - 12 verify that the captured optimal solution (marked in Fig. 12) corresponds to the lowest life cycle cost. In order to the analysis of optimal TSS and BSS design for different sizes of PV system, it is necessary to consider the whole costs of PV system within LCC. The average cost of a PV system in Australia is about $1.09/W [4]. Two percent of the initial cost of PV system is considered as the annual operational and maintenance costs. Four PV sizes are chosen and results are presented in Table 6. The optimal BSS and TSS sizes for different PV sizes show that increasing the size of PV increases the size of storage systems, while,

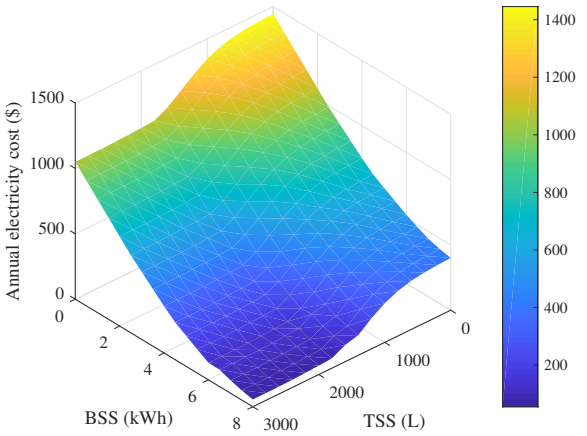

Figure 9: Sensitivity analysis of annual electricity cost.

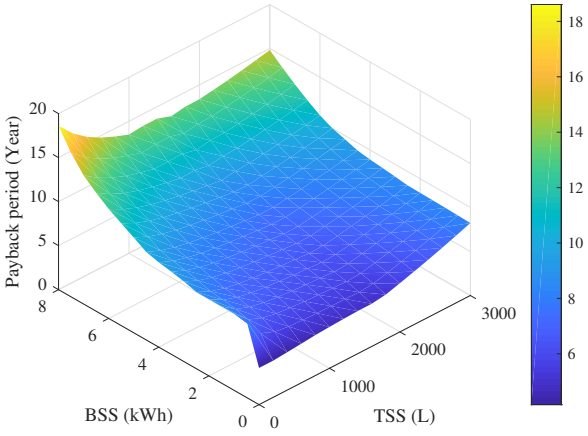

Figure 10: Sensitivity analysis of payback period.

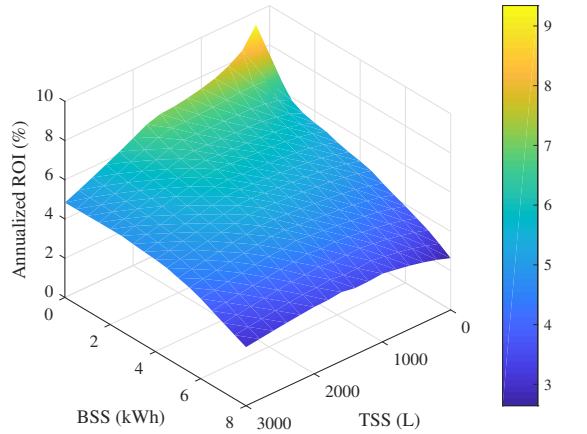

Figure 11: Sensitivity analysis of return on investment.

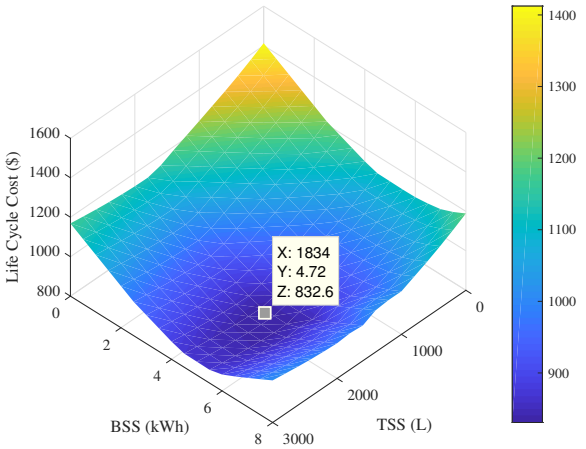

Figure 12: Sensitivity analysis of life cycle costs.

Table 6: OBTS results for different PV sizes.

PV size	kWp	2	4	6	8
TSS size	Liter	1200	1700	2200	2200
BSS size	kWh	3.4	4.2	5.0	5.2
Annual PV power	kWh	3380	6760	10140	13520
PV self-consumption	kWh	2984	4042	4708	4830
Annual electricity cost	$	958	396	233	195
LCC*	$	1464	1139	1206	1311
Payback period*	year	6.6	6.9	8.6	10.2
AROI*	%	5.4	5.2	4.2	3.4

* The life cycle cost of PV system is considered in LCC, payback period, and AROI.

the trend is not linear. The optimal sizes of TSS and BSS are required for taking advantage of PV generation in the higher size of PV. It is not economical to increase the storage sizes due to i) rising initial costs of PV, TSS and BSS which leads to increase the LCC, and ii) the sizes of TSS and BSS are mostly limited by households load.

The seasonal performance factor (SPF) on the ground source heat pump is 4.4 in heating mode and 4.8 in cooling mode for the optimal TSS size. In this work, increasing the temperature of the TSS has not been considered to increase PV self-consumption. Additionally, TSS is considered to be correctly insulated. OBTS optimizes the stored thermal energy in TSS to supply daily thermal demand and avoid tank heat loss. Therefore, different sizes of TSS do not significantly impact the SPF of HP. However, the higher sizes of TSS decreases the SPF slightly due to the increasing tank heat loss.

5.2. Experimental Validation of SBEMS

Fig. 13 shows the SELAB at Edith Cowan University, Western Australia. Experimental validations have been performed for the thermal and electrical energy systems installed at the SELAB. The thermal system consists of 3×1000 liters stainless steel tank (100 mm insulation layer), and ground source HP with 10.3 kW heating capacity and 7.1 kW cooling capacity (the power consumption of the HP is between 1.5-2 kW). The electrical system encompasses 12×285 W series mono-crystalline PV modules (3.5 kWp), 6×250 W series poly-crystalline PV modules (1.5 kWp), and $4 \times 4 \times 12$ V series lead-acid batteries modules MP12200 GEL CELL with a nominal voltage of 48 V and total capacity of 4×4.8 kWh. All home appliances, except the HP, are modeled as uncontrollable loads. The base load is the data of a smart meter for a house in Perth, Australia, as shown in Fig. 15b. The experiments are performed at SELAB with the operating constraints shown in Table 4. TSS is set to $m_{TSS} = 0.1$ m^3 in the first time step. The stored chilled/hot water volume in TSS is calculated by measuring the difference between the inlet and outlet water flow rates of the TSS. The indoor temperature set-point is considered between 22 °C and 24 °C. Fig. 14 shows the real-time pricing profile used in this study. This profile is based on wholesale electricity market from the Australian energy market operator (AEMO) website [4]. The RTP is for

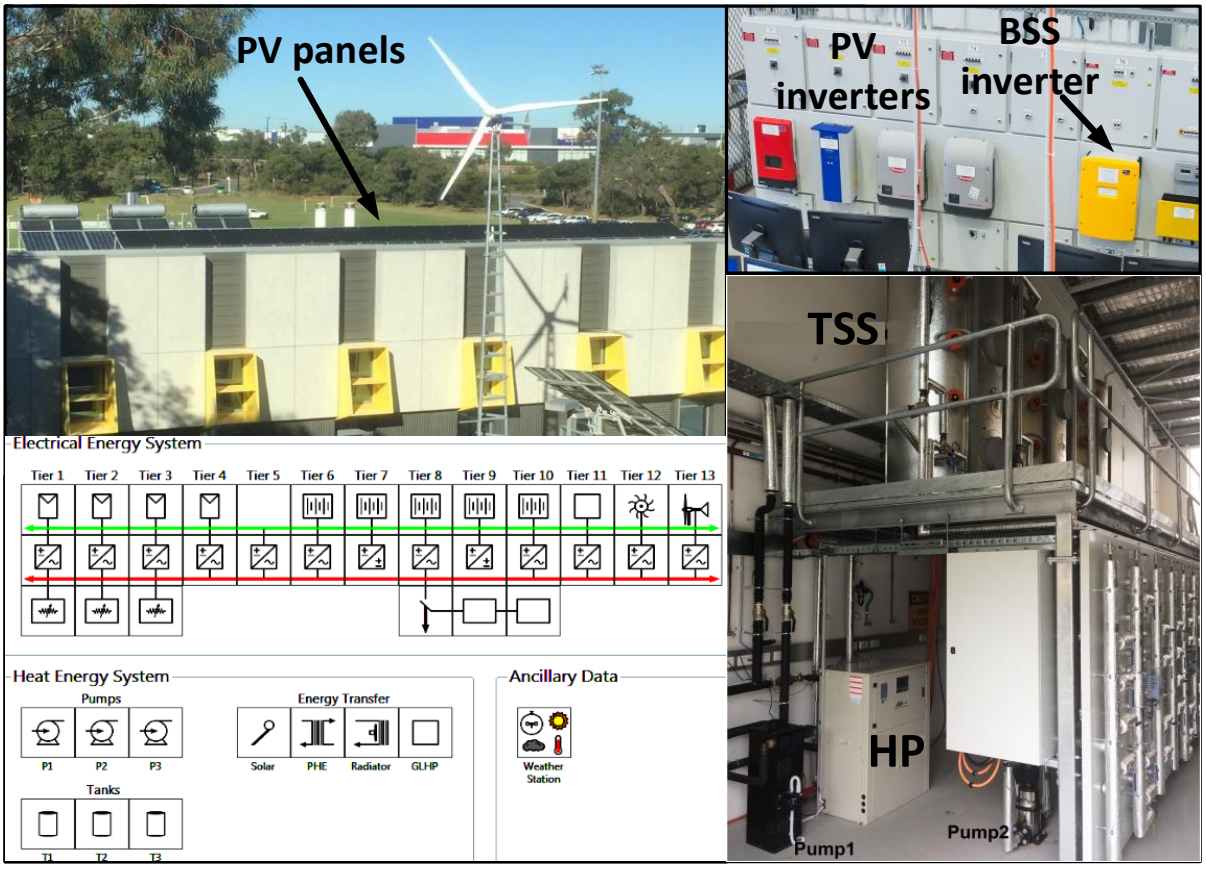

Figure 13: Smart Energy Laboratory (SELAB) at Edith Cowan University (ECU), Western Australia.

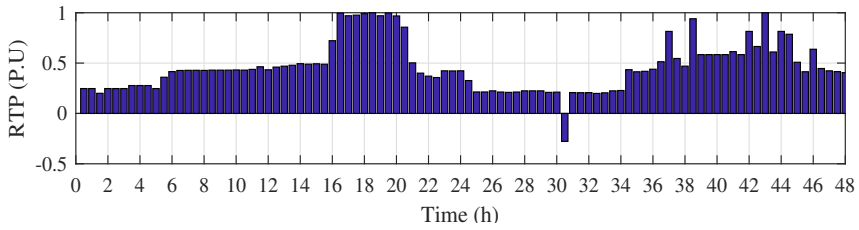

Figure 14: Wholesale electricity market price for two days in Jan-2019 [4].

two typical days in January 2019. A horizon prediction of $N = 24$h and a control sampling time of 5 min are chosen in this test. The proposed algorithm shifts the HP load based on RTP tariff and availability of PV generation, taking into account the stored thermal energy in the TSS (m_{TSS}) and the battery SOC. To verify the SBEMS results by experimental tests, TSS with the volume of 2000 liters and BSS with the capacity of 4.8 kWh are used as installed in SELAB.

Fig. 15 shows SBEMS results of two days in summer which these results obtain based on the actual system. Based on weather prediction, SBEMS calculates PV production and

thermal demand over the prediction horizon. In each time step, the indoor temperature is predicted and thermostat signal $\mathbb{U}$ determines the total required thermal demand of the building for the next time step (Fig. 15f). The SBEMS optimizes to run HP at midnight to directly supply thermal demand (Fig. 15c). Fig. 15d shows that SBEMS is applied to import power from the grid during midnight to avoid deep BSS discharging in the early morning. In second day, SBEMS runs the HP when the real-time price is negative. The power is also imported from the grid when the price is negative. It is assumed the SOC of battery is 50% in the first time step. Fig. 15e shows that the battery is charged by the grid power during low electricity price-period, based on RTP which has shown in Fig. 14, to supply base load and HP load during midnight and early morning. Then, BSS is fully charged by PV power to supply the load during peak-load hours (Fig. 15a). Fig. 15e also demonstrates HP is operated to charge TSS in midnight and when PV generation is sufficient to charge battery as well as supply the total load. The results show that according to m_{TSS}, the HP is run in the midday when the PV power is available; to increase stored chilled water m_{TSS}. The thermal demand is then supplied by TSS during peak-load hours.

To show the effectiveness of SBEMS, a test is done for the PV system without BSS and TSS. Figs. 16 and 17 show the experimental results of power dispatch for the system without the storage and with TSS and BSS, respectively. The HP load causes an increase in the total load during peak-load hours when the electricity price is high. This is due to the lack of storage systems. Thus, the total purchased grid power is 10.81 kWh in base case while it is decreased to 3.16 kWh, in the presence of TSS and BSS. In addition, the electricity cost is decreased by 84% from \$8.4 to \$1.3. The PV self-consumption is increased from 14.38 kWh (35.6 %) to 19.81 kWh (49.1 %).

Fig. 18 and Table 7 show the comparison between the model results and the experimental measurements. Fig. 18 demonstrates that the experimental measurements of BSS power and the grid power verify the simulation results with minor differences. Table 7 shows the PV power, PV self-consumption, HP electrical load, and the grid power for the first day for both simulations and measurements. The difference between the experimental results and the simulation results is mainly due to the 5-min time step. It can be seen that the results have verified the effectiveness of the proposed model. However, Table 7 shows 0.5 kWh difference in HP power consumption. This difference is due to the ground circulation pump of the ground source heat pump. The ground circulation pump operates about 2 min earlier than the HP and turns off 2 min after turning off the HP.

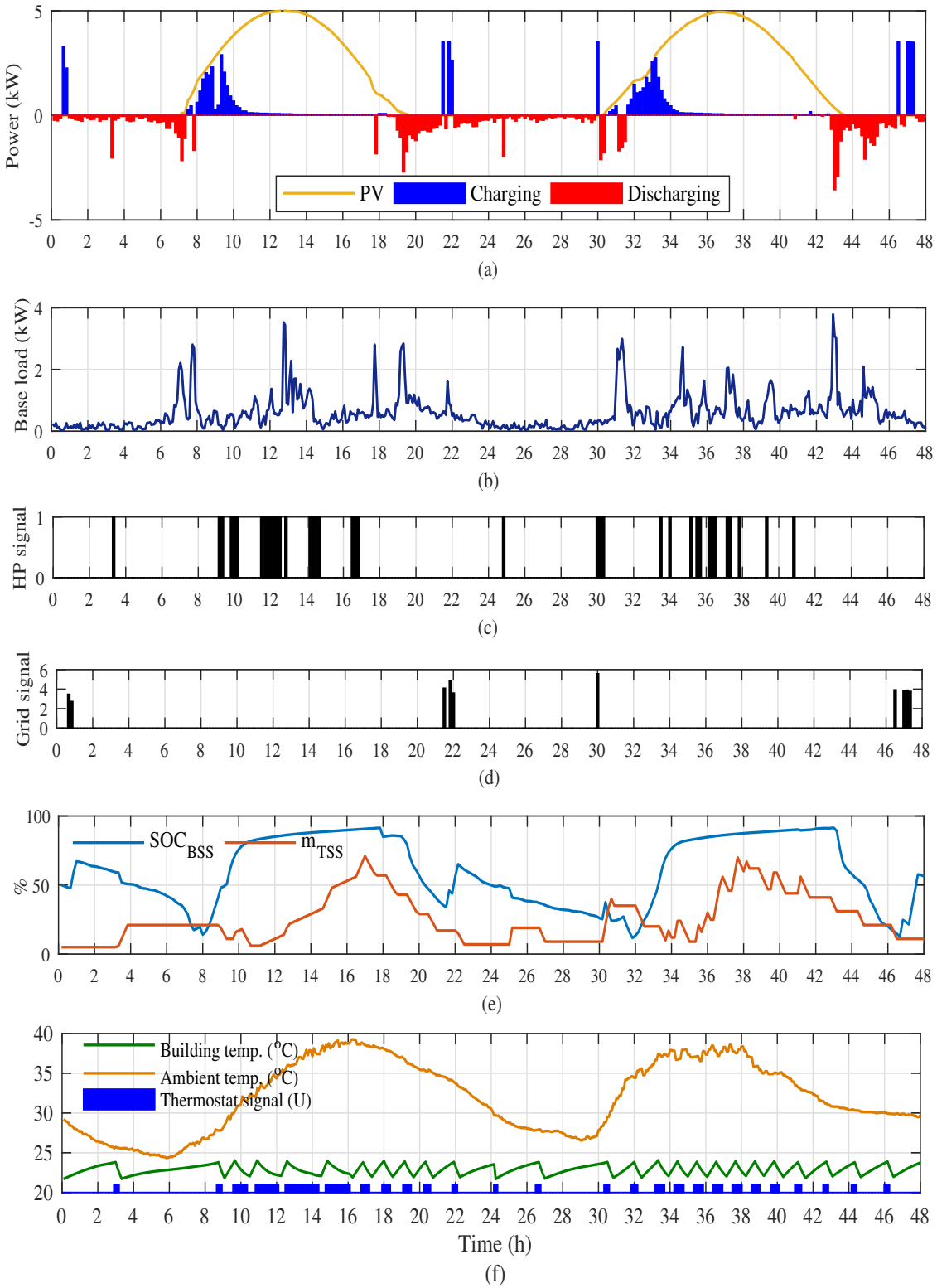

Figure 15: Power dispatch for a day in summer with the 4.8 kWh BSS and 2000 liters TSS. (a) PV production and battery power flow. (b) Base load. (c) HP operation signal. (d) Signal of imported power from the grid. (e) Percentages of the stored electrical and thermal energy in BSS and TSS. (f) Building temperature control result based on weather condition.

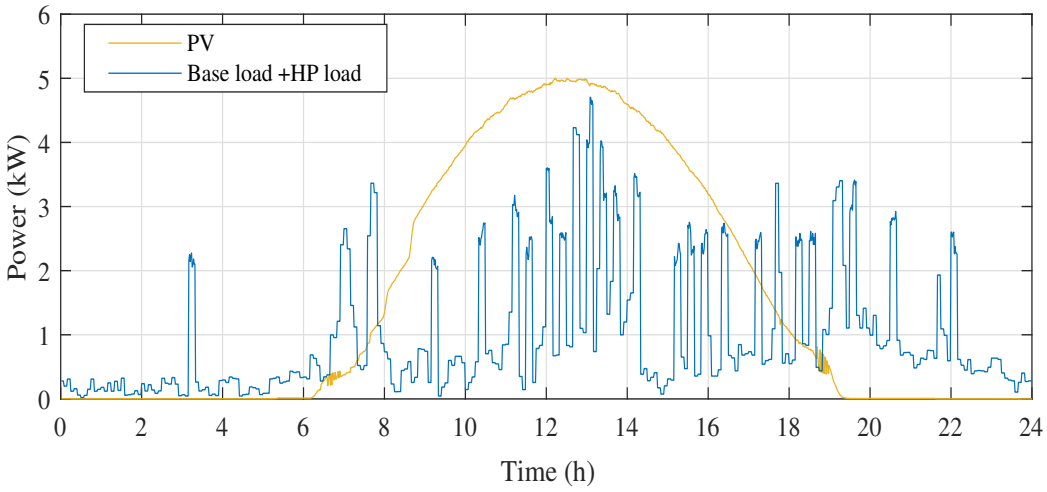

Figure 16: Experimental results of power dispatch for the PV system without the BSS and TSS.

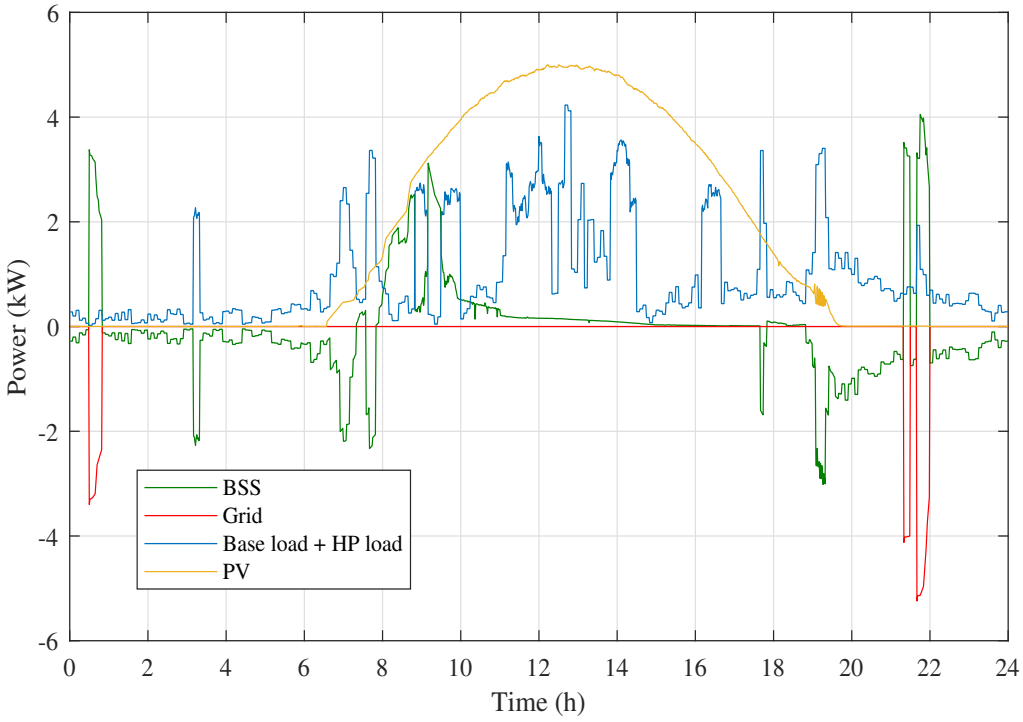

Figure 17: Experimental results of power dispatch for the PV system with 4.8 kWh BSS and 2000 liters TSS.

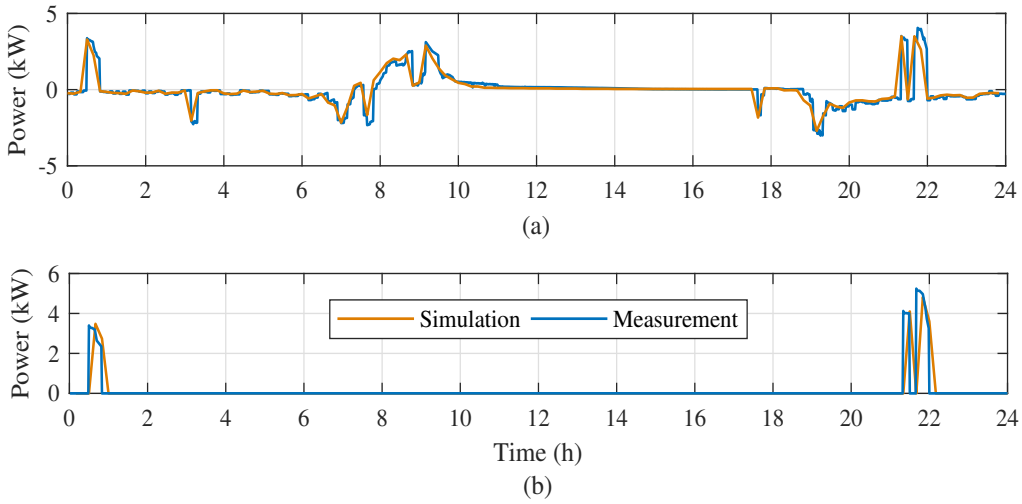

Figure 18: Comparison of experimental measurements and simulation results. (a) BSS power. (b) grid power.

Table 7: Comparison of experimental measurements and simulation results.

		Simulation	Experiment
PV power	kWh	38.4	39.3
PV self-consumption	kWh	19.6	20.1
HP load	kWh	12.1	12.6
Grid power	kWh	3.16	3.19

6. Conclusion

This paper presents a cost-effective framework for energy management of residential buildings with rooftop PVs, heat pumps (HPs), and thermal storage system (TSS) and battery storage system (BSS). Two methods are proposed and tested: 1) optimal BSS and TSS sizing (OBTS) to determine the optimal sizes of BSS and TSS, and 2) a smart building energy management system (SBEMS) to manage real-time operation of storage systems based on the OBTS results. The performance of OBTS and SBEMS are verified using detailed simulations and experimental tests. In addition, the cost benefits of the proposed OBTS are demonstrated for different scenarios by oversizing and undersizing both TSS and BSS components. The key outcomes of this study can be described as follows:

- The proposed OBTS reveals significant economic benefits in smart buildings with rooftop PVs by introducing BSS and TSS systems coupled with the HP. The results demonstrate that buildings with TSS only are a low investment solution in terms of short payback period and reasonable AROI. However, buildings with either thermal or battery storage (Table 5, Cases II and III) are not as cost-effective as the proposed TSS+BSS systems of Case IV, in terms of low annual electricity and life cycle costs. In particular, the control of residential HP coupled with TSS reduces building demand

from peak-load hours. Consequently, the BSS size is decreased. Accordingly, thermal and battery storage systems significantly increase PV self-consumption.

- With optimal sizing of BSS and TSS, the proposed SBEMS significantly reduces the total electricity cost of the smart building by shifting the HP loads based on DRP. This is done by charging the battery either during low-price electricity hours or when PV power is available.

The results of this paper demonstrate that residential rooftop PV systems can rely on HPs coupled with TSS systems as shifting technologies to avoid power system challenges caused by exporting excess PV power to the grid. The enhanced system can significantly reduce the burden of residential loads at peak hours by increasing rooftop PV self-consumption. Due to the high initial investment and operating costs of BSS, adding TSS to air-conditioning systems is more economical since end-users can take full advantage of rooftop PV systems with a reasonable investment cost. Accordingly, distribution network operators can support customers by introducing an incentive framework to foster HP systems. The proposed framework can be modified to consider the power sharing within buildings. It can also be applied in peer-to-peer trading with other types of HVAC systems and renewable energy resources.

Appendix A. HP heat transfer

Fig. 19 shows the schematic of heat transfer of the HP. The heat transfer equations in heating and cooling are as follows:

$$\dot{Q}_{HP} = P_{HP} + \dot{Q}_e \tag{A.1}$$

$$\dot{Q}_{HP} + P_{HP} = \dot{Q}_e \tag{A.2}$$

where $\dot{Q}_{HP}$ is determined by consumed power by the compressor and the heat taken (given) from (to) the environment ($\dot{Q}_e$).

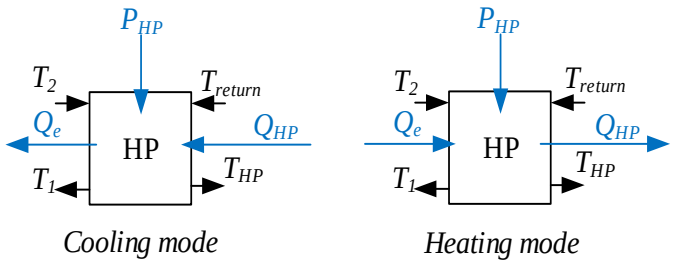

Figure A.19: Heat transfer for HP system.

The COP depends on temperature difference between external source and internal source. The characteristics of COP can be explained by ideal Carnot heat pump cycle [4].

$$COP_h = \eta \cdot \frac{(T_e - \delta T)}{(T_{HP} + \delta T) - (T_e - \delta T)} + 1 \tag{A.3}$$

where $\eta = 0.55$ is the Carnot efficiency, $\delta T = 5^oC$ is the temperature difference of the heat exchangers, and T_e is the ground temperature which is 16^oC in WA.

The modeled HP is a single phase ground source heat pump from Mammoth [5]. The HP model is MSR L024H. The HP technical data are taken from the manufacture's datasheet ([5]) to evaluate the HP performance and power consumption.

Appendix B. Particle Swarm Optimization

PSO is a heuristic algorithm for solving complex optimization problems by a population (swarm) of named particles [5]. Each particle is a vector which consists of N decision variables and defines a position of the search space. During the iterations, each particle moves randomly based on the swarm's experience and its own best knowledge. Note that each particle moves toward the location of the current global best position (*pbest*) and the group's best experience (*gbest*). This process is repeated until the termination criterion is reached. In each iteration (t), the updating pattern of particles is given by:

$$v_j(t+1) = w(t) \times v_j(t) + c_1 \times r_1(pbest_j(t) - x_j(t)) + c_2 \times r_2(gbest_j(t) - x_j(t)) \tag{B.1}$$

$$x_j(t+1) = v_j(t+1) + x_j(t) \qquad (t = 1, 2, ..., t_{max}) \tag{B.2}$$

where x_j and v_j are the position and the velocity of jth particle, respectively. $j = 1, 2, ..., N_p$ is the index of particle, N_p is the size of particle, r_1 and r_2 represent uniform random numbers between 0 and 1 which are independently generated for each particle in each update, c_1 and c_2 represent learning factors which are usually between 0 and 2, t_{max} is the maximum iteration times and w is the inertia constant.

References

[1] REN21-Secretariat, Renewables 2018 global status report (2018).
URL `http://www.ren21.net/gsr-2018/`

[2] K. M. Tsui, S.-C. Chan, Demand response optimization for smart home scheduling under real-time pricing, IEEE Transactions on Smart Grid 3 (4) (2012) 1812–1821.

[3] Z. Moghaddam, I. Ahmad, D. Habibi, M. A. Masoum, A coordinated dynamic pricing model for electric vehicle charging stations, IEEE Transactions on Transportation Electrification 5 (1) (2019) 226–238.

[4] C. K. Das, O. Bass, G. Kothapalli, T. S. Mahmoud, D. Habibi, Overview of energy storage systems in distribution networks: Placement, sizing, operation, and power quality, Renewable and Sustainable Energy Reviews 91 (2018) 1205–1230.

[5] A. Baniasadi, D. Habibi, O. Bass, M. A. S. Masoum, Optimal real-time residential thermal energy management for peak-load shifting with experimental verification, IEEE Transactions on Smart Grid (2018) 1–1.

[6] Y. Kim, Optimal price-based demand response of hvac systems in multi-zone office buildings considering thermal preferences of individual occupants, IEEE Transactions on Industrial Informatics (2018).

[7] M. Shabani, J. Mahmoudimehr, Techno-economic role of pv tracking technology in a hybrid pv-hydroelectric standalone power system, Applied energy 212 (2018) 84–108.

[8] N. Mousavi, G. Kothapalli, D. Habibi, M. Khiadani, C. K. Das, An improved mathematical model for a pumped hydro storage system considering electrical, mechanical, and hydraulic losses, Applied Energy 247 (2019) 228–236.

[9] N. Mousavi, G. Kothapalli, D. Habibi, C. K. Das, Operational cost reduction of pv-phs systems in farmhouses: Modelling, design, and experimental validation, in: IOP Conference Series: Earth and Environmental Science, Vol. 322, IOP Publishing, 2019, p. 012011.

[10] G. Yang, M. Chen, The methodology for size optimization of the photovoltaic/wind hybrid system, Energy Sources, Part A: Recovery, Utilization, and Environmental Effects 32 (17) (2010) 1644–1650.

[11] G. Mokhtari, G. Nourbakhsh, A. Gosh, Optimal sizing of combined pv-energy storage for a grid-connected residential building, Advances in Energy Engineering 1 (3) (2013) 53–65.

[12] T. K. Brekken, A. Yokochi, A. Von Jouanne, Z. Z. Yen, H. M. Hapke, D. A. Halamay, Optimal energy storage sizing and control for wind power applications, IEEE Transactions on Sustainable Energy 2 (1) (2010) 69–77.

[13] D. Parra, M. Gillott, S. A. Norman, G. S. Walker, Optimum community energy storage system for pv energy time-shift, Applied Energy 137 (2015) 576–587.

[14] F. Benavente, A. Lundblad, P. E. Campana, Y. Zhang, S. Cabrera, G. Lindbergh, Photovoltaic/battery system sizing for rural electrification in bolivia: Considering the suppressed demand effect, Applied energy 235 (2019) 519–528.

[15] X. Wu, X. Hu, X. Yin, C. Zhang, S. Qian, Optimal battery sizing of smart home via convex programming, Energy 140 (2017) 444–453.

[16] R. Hemmati, H. Saboori, Stochastic optimal battery storage sizing and scheduling in home energy management systems equipped with solar photovoltaic panels, Energy and Buildings 152 (2017) 290–300.

[17] O. Talent, H. Du, Optimal sizing and energy scheduling of photovoltaic-battery systems under different tariff structures, Renewable energy 129 (2018) 513–526.

[18] O. Erdinc, N. G. Paterakis, I. N. Pappi, A. G. Bakirtzis, J. P. Catalão, A new perspective for sizing of distributed generation and energy storage for smart households under demand response, Applied Energy 143 (2015) 26–37.

[19] R. Atia, N. Yamada, Sizing and analysis of renewable energy and battery systems in residential microgrids, IEEE Transactions on Smart Grid 7 (3) (2016) 1204–1213.

[20] J. Koskela, A. Rautiainen, P. Järventausta, Using electrical energy storage in residential buildings–sizing of battery and photovoltaic panels based on electricity cost optimization, Applied Energy 239 (2019) 1175–1189.

[21] T. Beck, H. Kondziella, G. Huard, T. Bruckner, Optimal operation, configuration and sizing of generation and storage technologies for residential heat pump systems in the spotlight of self-consumption of photovoltaic electricity, Applied energy 188 (2017) 604–619.

[22] D. Fischer, K. B. Lindberg, H. Madani, C. Wittwer, Impact of pv and variable prices on optimal system sizing for heat pumps and thermal storage, Energy and Buildings 128 (2016) 723–733.

[23] M. Kharseh, H. Wallbaum, The effect of different working parameters on the optimal size of a battery for grid-connected pv systems, Energy Procedia 122 (2017) 595–600.

[24] L. Zhou, Y. Zhang, X. Lin, C. Li, Z. Cai, P. Yang, Optimal sizing of pv and bess for a smart household considering different price mechanisms, IEEE access 6 (2018) 41050–41059.

[25] B. Boeckl, T. Kienberger, Sizing of pv storage systems for different household types, Journal of Energy Storage 24 (2019) 100763.

[26] D. Wu, M. Kintner-Meyer, T. Yang, P. Balducci, Analytical sizing methods for behind-the-meter battery storage, Journal of Energy Storage 12 (2017) 297–304.

[27] J. von Appen, Incentive design, sizing and grid integration of residential pv systems with heat pumps and battery storage systems, in: 2018 15th International Conference on the European Energy Market (EEM), IEEE, 2018, pp. 1–5.

[28] J. von Appen, M. Braun, Sizing and improved grid integration of residential pv systems with heat pumps and battery storage systems, IEEE Transactions on Energy Conversion 34 (1) (2019) 562–571.

[29] G. Angenendt, S. Zurmühlen, F. Rücker, H. Axelsen, D. U. Sauer, Optimization and operation of integrated homes with photovoltaic battery energy storage systems and power-to-heat coupling, Energy Conversion and Management: X 1 (2019) 100005.

[30] P. Huang, M. Lovati, X. Zhang, C. Bales, S. Hallbeck, A. Becker, H. Bergqvist, J. Hedberg, L. Maturi, Transforming a residential building cluster into electricity prosumers in sweden: Optimal design of a coupled pv-heat pump-thermal storage-electric vehicle system, Applied Energy 255 (2019) 113864.

[31] M. Lovati, G. Salvalai, G. Fratus, L. Maturi, R. Albatici, D. Moser, New method for the early design of bipv with electric storage: A case study in northern italy, Sustainable Cities and Society 48 (2019) 101400.

[32] M. I. Hlal, V. K. Ramachandaramurthy, A. Sarhan, A. Pouryekta, U. Subramaniam, Optimum battery depth of discharge for off-grid solar pv/battery system, Journal of Energy Storage 26 (2019) 100999.

[33] S. Chen, H. B. Gooi, M. Wang, Sizing of energy storage for microgrids, IEEE Transactions on Smart Grid 3 (1) (2012) 142–151.

[34] A. Marszal-Pomianowska, P. Heiselberg, O. K. Larsen, Household electricity demand profiles–a high-resolution load model to facilitate modelling of energy flexible buildings, Energy 103 (2016) 487–501.

[35] A. Baniasadi, D. Habibi, W. Al-Saedi, M. A. S. Masoum, A cost-effective thermal and electrical energy storage management strategy for smart buildings, in: 2019 IEEE PES Innovative Smart Grid Technologies Europe (ISGT-Europe), 2019, pp. 1–5. doi:10.1109/ISGTEurope.2019.8905537.

[36] D. Molina, C. Lu, V. Sherman, R. G. Harley, Model predictive and genetic algorithm-based optimization of residential temperature control in the presence of time-varying electricity prices, IEEE Transactions on Industry Applications 49 (3) (2013) 1137–1145.

[37] E. Vrettos, E. C. Kara, J. MacDonald, G. Andersson, D. S. Callaway, Experimental demonstration of frequency regulation by commercial buildings- part i: Modeling and hierarchical control design, IEEE Transactions on Smart Grid (2017) 1–1.

[38] I. Staffell, D. Brett, N. Brandon, A. Hawkes, A review of domestic heat pumps, Energy & Environmental Science 5 (11) (2012) 9291–9306.

[39] Western australian electricity generator and retailer corporation., `https://www.synergy.net.au/Your-home/Energy-plans/Smart-Home-Plan`, accessed: 2019-04-19.

[40] B. Xu, A. Oudalov, A. Ulbig, G. Andersson, D. S. Kirschen, Modeling of lithium-ion battery degradation for cell life assessment, IEEE Transactions on Smart Grid 9 (2) (2018) 1131–1140.

[41] D. U. Sauer, H. Wenzl, Comparison of different approaches for lifetime prediction of electrochemical systems using lead-acid batteries as example, Journal of Power sources 176 (2) (2008) 534–546.

[42] N. Omar, M. A. Monem, Y. Firouz, J. Salminen, J. Smekens, O. Hegazy, H. Gaulous, G. Mulder, P. Van den Bossche, T. Coosemans, et al., Lithium iron phosphate based battery–assessment of the aging parameters and development of cycle life model, Applied Energy 113 (2014) 1575–1585.

[43] https://www.solarquotes.com.au/battery-storage/comparison-table/, accessed: 2019.

[44] N. Ming, W. Can, X. Zhao, A review on applications of heuristic optimization algorithms for optimal power flow in modern power systems, Journal of Modern Power Systems and Clean Energy 2 (4) (2014) 289–297.

[45] M. Killian, M. Kozek, Ten questions concerning model predictive control for energy efficient buildings, Building and Environment 105 (2016) 403–412.

[46] K. Feldman, T. Jazouli, P. A. Sandborn, A methodology for determining the return on investment associated with prognostics and health management, IEEE Transactions on Reliability 58 (2) (2009) 305–316.

[47] https://www.solarchoice.net.au/blog/solar-power-system-prices, accessed: 2019.

[48] Australian energy market operator, https://www.aemo.com.au/, accessed: 2019-01-03.

[49] J. Salpakari, T. Rasku, J. Lindgren, P. D. Lund, Flexibility of electric vehicles and space heating in net zero energy houses: an optimal control model with thermal dynamics and battery degradation, Applied energy 190 (2017) 800–812.

[50] Water source heat pump (package type e series) 3.0kw-20.1kw (50hz)., https://www.academia.edu/16499984/Mammoth_WSHP_Package_E_series_50HZ_R410A_catalogue_1_, accessed: 2019-10-19.

[51] W. Al-Saedi, S. W. Lachowicz, D. Habibi, O. Bass, Power flow control in grid-connected microgrid operation using particle swarm optimization under variable load conditions, International Journal of Electrical Power & Energy Systems 49 (2013) 76–85.